Feedback Control Design for Drive Shaft Vibration Suppression Based on Frequency Domain Analysis of Two-Input-Two-Output Motor Drive System

Guangzhi Yu, Hiroyuki Fuse, Hiroshi Fujimoto
The University of Tokyo
5-1-5, Kashiwanoha, Kashiwa,
Chiba, 277-8561, Japan
Email: yu.guangzhi21@ae.k.u-tokyo.ac.jp

Kaoru Sawase, Naoki Takahashi, Ryota Takahashi,
Yutaro Okamura, Ryosuke Koga
MITSUBISHI MOTORS CORPORATION
1, Nakashinkiri, Hashimecho, Okazaki,
Aichi, 444–8501, Japan

***Abstract*—To improve the cornering performance of the vehicle, the two-motor-torque difference amplification-torque vectoring differential (TDA-TVD) has been proposed for the two-input- two-output motor drive system, since it enables to increase the maximum torque difference between left and right wheels. However, this mechanism has problems of torque coupling and vibration in left and right drive shafts. In the previous research conducted by the authors, the TDA-TVD model analysis and drive shaft vibration suppression control methods are provided, but only feedforward control is considered. In this paper, a drive shaft vibration suppression controller is designed with frequency domain analysis of the model. The proposed controller consists of a feedforward controller using the inverse model of TDA-TVD, and a feedback controller using the rotation speed of the motor. The experimental evaluation of the proposed controller is performed using a real vehicle with the TDA-TVD system.**

***Index Terms*—Electric vehicle, motor drive system, two-input-two-output system, torque vectoring differential, vibration suppression control, anti-jerk control, frequency domain feedback control design**

I. Introduction

Due to the effects of global warming, the regulations on gasoline and diesel vehicles have been tighten. The research on electric vehicles has become increasingly important because they do not emit greenhouse gas while driving. In addition, there are three other important characteristics of electric vehicles: 1) each wheel can be controlled independently by the distributed arrangement of driving motors; 2) motor torque can be estimated by the current of motors; and 3) torque response of motors is about 100 times faster than internal combustion engines. By utilizing these characteristics, advanced motion control of the electric vehicle becomes possible [1], [2].

To improve the cornering performance of the vehicle, distributed arrangement of driving motors has been studied [3]. Fig. 1 shows the distributed arrangement of the rear driving system. It is thought in-wheel motor deteriorates the ride comfort due to the increase in unsprung weight. However, the vertical vibration of the vehicle can be suppressed by using the reaction force of the suspension and motor torque [4], [5]. The driving system with on-board motor has torsional resonance in low frequency band due to the elasticity of the drive shaft. Different from gasoline and diesel vehicles, electric vehicles can suppress this vibration by shaping the motor torque command actively [6]–[10].

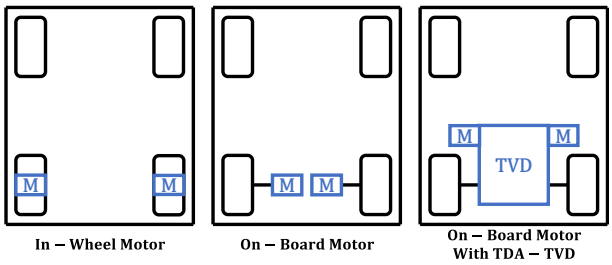

Fig. 1. Distributed arrangement of the rear driving system.

However, this problem becomes more complicated in the two-motor-torque difference amplification-torque vectoring differential (TDA-TVD). The TDA-TVD has been proposed for two-input-two-output motor drive system, because it can increase the maximum torque difference between left and right wheels, but there is torque coupling between left and right drive shafts. In the previous research conducted by the authors, the TDA-TVD model is analyzed in the time domain and the drive shaft vibration is suppressed by a feedforward controller with a decoupling compensator. However, the drive shaft torque possibly vibrates while the vehicle is turning, because the controller does not consider the cornering model in load side [11]. Another previous research of the authors provides a frequency domain analysis and a feedforward vibration suppression controller with the inverse model of TDA-TVD. The controller considers the cornering model, but does not consider the vibration caused by modeling error and disturbance [12]. In this paper, a drive shaft vibration suppression controller is designed with the frequency domain analysis of the model. The proposed controller consists of a feedforward controller using the inverse model of TDA-TVD, and a feedback controller using the rotation speed of the motor. The effectiveness of drive shaft vibration suppression controller is evaluated by an acceleration experiment using a real vehicle with the TDA-TVD system.

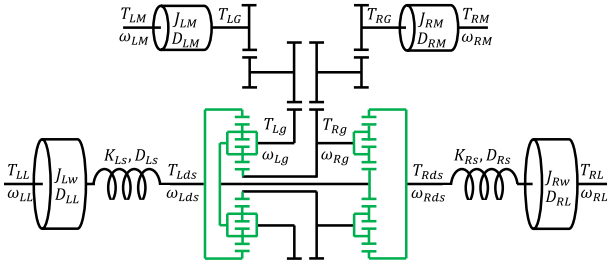

Fig. 2. Schematic diagram of TDA-TVD [13]. TDA-TVD has a mechanical coupling between left and right drive shafts through planetary gears.

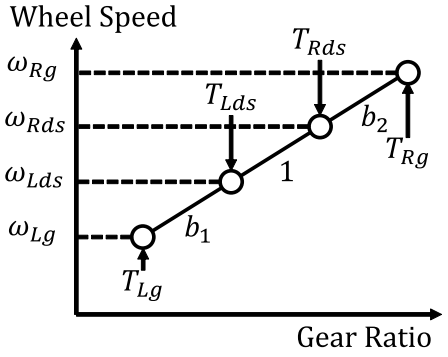

Fig. 3. Velocity diagram of TDA-TVD [13]. The relationship of torque and rotation speed in left and right sides can be visually represented.

II. Dynamic model of TDA-TVD

A. Normal mode

Fig. 2 shows the schematic diagram of TDA-TVD [13]. Fig. 3 shows the velocity diagram of TDA-TVD [13]. Where T_M is motor torque, ω_M is motor rotation speed, J_M is motor inertia, D_M is motor damping factor, ω_g is reduction gear rotation speed ($\omega_g = \omega_M/N_g$), T_g is reduction gear torque ($T_g = T_M N_g$), N_g is first reduction gear ratio, b_1, b_2 are second reduction gear ratio, ω_{ds} is drive shaft rotation speed, T_{ds} is drive shaft torque, K_s is drive shaft stiffness, D_s is drive shaft damping factor, ω_L is wheel rotation speed, J_w is wheel inertia, D_L is wheel damping factor, T_L is load torque, subscript R and L are right and left sides.

J_L is assumed as the nominal inertia of the wheel at the nominal slip ratio λ_n. The nonlinear dynamic load model can be linearized as the following equations [9], [14].

$$J_L = J_w + \frac{Mr^2}{2}(1-\lambda_n), \tag{1}$$

$$\omega_L = \frac{1}{J_L s + D_L} T_{ds}, \tag{2}$$

where M is vehicle mass, r is wheel radius. $\lambda_n = 0$ and the vehicle is driven by two rear wheels in this paper.

The linear model block diagram of TDA-TVD is shown in Fig. 4. The transfer function from $\boldsymbol{T}_M$ to $\boldsymbol{\omega}_M$ is expressed as the following equation.

$$\begin{aligned}\boldsymbol{\omega}_M &= \left[\boldsymbol{E} + \boldsymbol{P}_M \boldsymbol{N}_g^{-1}\left(\boldsymbol{B}^T\right)^{-1}\left(\boldsymbol{P}_{DS}^{-1} + \boldsymbol{P}_L\right)^{-1}\boldsymbol{B}^{-1}\boldsymbol{N}_g^{-1}\right]^{-1}\boldsymbol{P}_M\boldsymbol{T}_M \\ &= \begin{bmatrix}\omega_{RM}/T_{RM} & \omega_{RM}/T_{LM} \\ \omega_{LM}/T_{RM} & \omega_{LM}/T_{LM}\end{bmatrix}\boldsymbol{T}_M,\end{aligned} \tag{3}$$

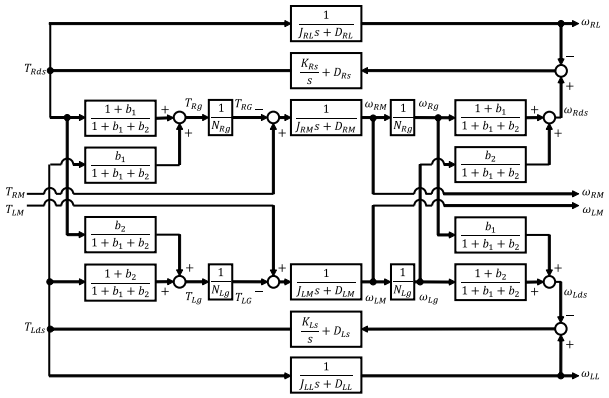

Fig. 4. Block diagram of TDA-TVD.

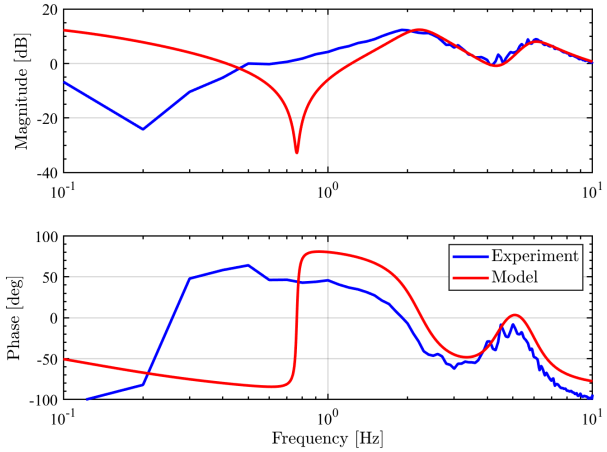

Fig. 5. Frequency response of $\frac{\omega_{LM}}{T_{LM}}$. The controller design becomes difficult, because there are two resonances at 2 Hz and 6 Hz in this coupling model.

where $\boldsymbol{E} = \begin{bmatrix}1 & 0\\ 0 & 1\end{bmatrix}$, $\boldsymbol{B} = \begin{bmatrix}1+b_2 & -b_2\\ -b_1 & 1+b_1\end{bmatrix}$,

$$\boldsymbol{\omega}_M = \begin{bmatrix}\omega_{RM}\\ \omega_{LM}\end{bmatrix},\ \boldsymbol{P}_M = \begin{bmatrix}1/(J_{RM}s + D_{RM}) & 0\\ 0 & 1/(J_{LM}s + D_{LM})\end{bmatrix},$$

$$\boldsymbol{N}_g = \begin{bmatrix}N_{Rg} & 0\\ 0 & N_{Lg}\end{bmatrix},\ \boldsymbol{P}_{DS} = \begin{bmatrix}K_{Rs}/s + D_{Rs} & 0\\ 0 & K_{Ls}/s + D_{Ls}\end{bmatrix},$$

$$\boldsymbol{T}_M = \begin{bmatrix}T_{RM}\\ T_{LM}\end{bmatrix},\ \boldsymbol{P}_L = \begin{bmatrix}1/(J_{RL}s + D_{RL}) & 0\\ 0 & 1/(J_{LL}s + D_{LL})\end{bmatrix}.$$

Fig. 5 shows the frequency response of $\frac{\omega_{LM}}{T_{LM}}$. The blue line of experimental data is obtained by the excitation using chirp signal chirp signals to motor torque command of TDA-TVD. The load side is reproduced with left and right independent dynamo bench by simulating the translation motion of the vehicle. The load inertia of the wheel corresponded to $\lambda_n = 0$ in equation (1). The controller has the risk of instability, because there are two resonances at 2 Hz and 6 Hz in this coupling model. The red line shows the result of model fitting by estimating the parameters in equation (3). There are some parameters fixed to the experimental parameters shown in TABLE I. The frequency response above 2 Hz is tuned to match the experimental data. Meanwhile, the frequency response below 2 Hz is different from experimental data because the relationship of left and right wheel when translation motion is not considered in this model.

TABLE I
EXPERIMENTAL PARAMETERS.

Parameter	Value
Vehicle mass M	2173 kg
Effective wheel radius r	0.338 m
Nominal slip ratio λ_n	0
Wheel inertia J_ω	1.813 kg m^2
Motor inertia J_M	0.018 kg m^2
First reduction gear ratio N_g	10.8
Second reduction gear ratio b_1 and b_2	0.892, 0.895

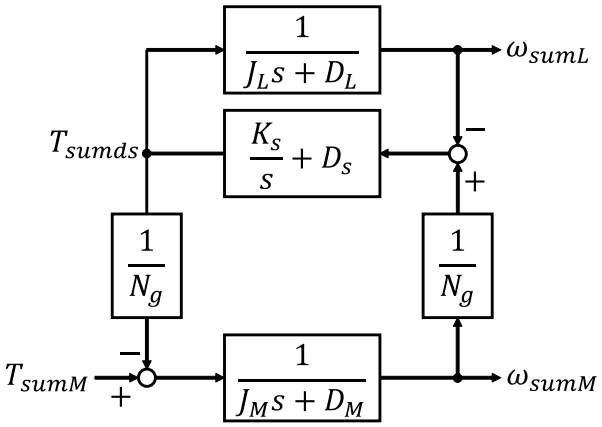

Fig. 6. Block diagram of summation mode.

B. Summation and differential modes

According to the previous research [12], the model of TDA-TVD is decoupled through summation and differential modes. The summation mode is translation motion of the vehicle, and in-phase torque is input to the left and right motors. The differential mode is yaw motion of the vehicle, and the reverse phase torque is input to the left and right motors. It is assumed that $b_1 = b_2 = b$, and all the parameters of left and right sides are the same. By performing the coordinate transformation of equations (4) and (5), the torque and rotation relationship between left and right sides become equation (6) in summation mode.

$$\begin{bmatrix} T_{sumM} & T_{sumds} \\ T_{difM} & T_{difds} \end{bmatrix} = \frac{1}{2}\begin{bmatrix} 1 & 1 \\ 1 & -1 \end{bmatrix}\begin{bmatrix} T_{RM} & T_{Rds} \\ T_{LM} & T_{Lds} \end{bmatrix}, \tag{4}$$

$$\begin{bmatrix} \omega_{sumM} & \omega_{sumL} \\ \omega_{difM} & \omega_{difL} \end{bmatrix} = \frac{1}{2}\begin{bmatrix} 1 & 1 \\ 1 & -1 \end{bmatrix}\begin{bmatrix} \omega_{RM} & \omega_{RL} \\ \omega_{LM} & \omega_{LL} \end{bmatrix}, \tag{5}$$

$$\begin{bmatrix} T_{Rg} & \omega_{Rds} \\ T_{Lg} & \omega_{Lds} \end{bmatrix} = \begin{bmatrix} 1 & 0 \\ 0 & 1 \end{bmatrix}\begin{bmatrix} T_{Rds} & \omega_{Rm} \\ T_{Lds} & \omega_{Lm} \end{bmatrix}. \tag{6}$$

Where the subscript *sum* and *dif* represent the summation and differential modes. Equation (6) means that the model of TDA-TVD is decoupled. The model of TDA-TVD becomes to the block diagram of summation mode shown in Fig. 6 using the linearization method in equation (1) and (2). In this paper, the controller is designed based on summation mode. By decoupling the model of TDA-TVD, the transfer function of $\frac{T_{sumds}}{T_{sumM}}$ and $\frac{\omega_{sumM}}{T_{sumM}}$ are expressed as follows.

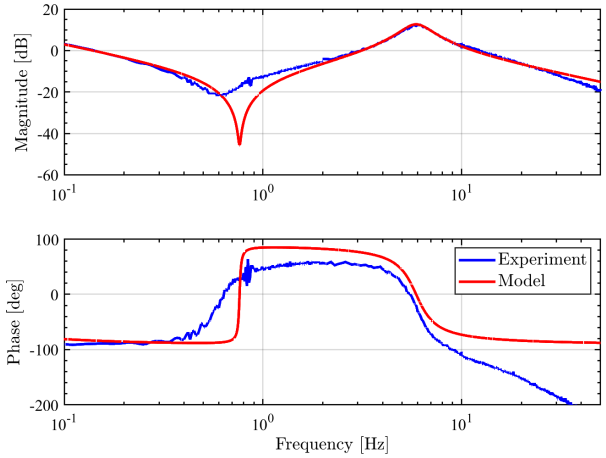

Fig. 7. Frequency response of $\frac{\omega_{sumM}}{T_{sumM}}$. There are a resonance and an anti-resonance in this model.

$$\begin{aligned} T_{sumds} &= \frac{N_g[J_L D_s s^2 + (J_L K_s + D_s D_L)s + K_s D_L]}{a_3 s^3 + a_2 s^2 + a_1 s + a_0} T_{sumM} \\ &= P_{sumSn}(s) T_{sumM}, \end{aligned} \tag{7}$$

$$\begin{aligned} \omega_{sumM} &= \frac{N_g^2[J_L s^2 + (D_L + D_s)s + K_s]}{a_3 s^3 + a_2 s^2 + a_1 s + a_0} T_{sumM} \\ &= P_{sumMn}(s) T_{sumM}, \end{aligned} \tag{8}$$

Where a_3 to a_0 in the transfer function are given by the following equations.

$$\begin{cases} a_3 = N_g^2 J_L J_M \\ a_2 = N_g^2(J_M D_L + J_M D_s + J_L D_M) + J_L D_s \\ a_1 = N_g^2(J_M K_s + D_L D_M + D_s D_M) + J_L K_s + D_L D_s \\ a_0 = N_g^2 K_s D_M + D_L K_s. \end{cases} \tag{9}$$

Fig. 7 shows the frequency response of $\frac{\omega_{sumM}}{T_{sumM}}$. The blue line of experimental data is obtained by the same method of normal mode. The frequency response of $\frac{\omega_{sumM}}{T_{sumM}}$ has a resonance at 6 Hz and an anti-resonance at 0.6 Hz. The red line shows the result of model fitting by estimating the parameters in equation (8). The mass line and resonance frequency are same with the experimental data, but the anti-resonance frequency is different from experimental data because there are some stiffness and damping factors not considered in the plant model. It is estimated that the reason of phase delay above 10 Hz could be communication delay and the rate limit of motor torque command.

III. DESIGN OF VIBRATION SUPPRESSION CONTROLLER FOR TDA-TVD

The block diagram of the drive shaft vibration suppression controller is shown in Fig. 8. The controller consists of a feedforward controller using the summation inverse model from motor torque to drive shaft torque, and a feedback controller using the drive shaft rotation speed.

A. Feedforward controller

The feedforward controller C_{sumFF} suppresses drive shaft vibration with the inverse model from T_{sumM} to T_{sumds} as the following equations [11], [12].

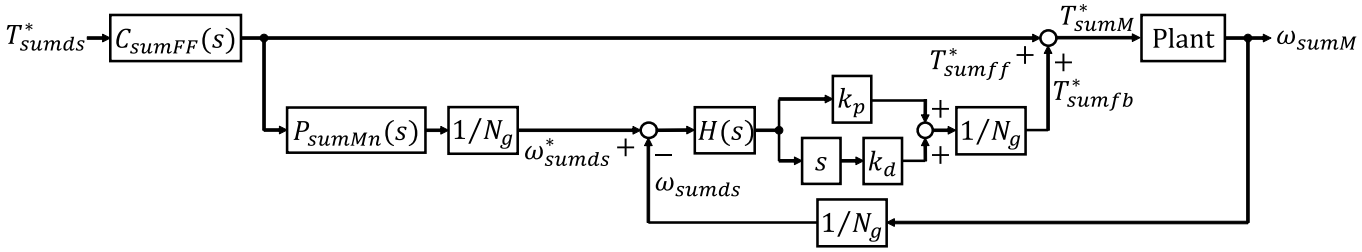

Fig. 8. Block diagram of the drive shaft vibration suppression controller. The controller consists of a feedforward controller using the summation inverse model from motor torque to drive shaft torque, and a feedback controller using the drive shaft rotation speed.

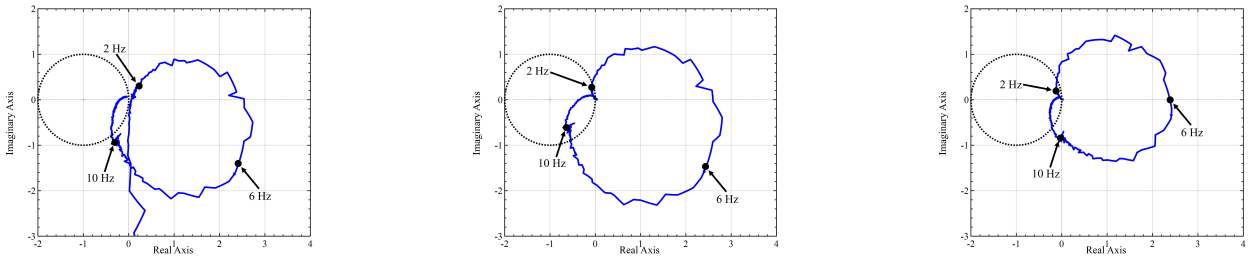

(a) P control. (b) P control with band-pass filter. (c) PD control with band-pass filter.

Fig. 9. Nyquist plots of controller design procedure. P control has the high magnitude below 2 Hz. P control with band-pass filter has phase delay above 10 Hz. PD control with band-pass filter decreases the magnitude below 2 Hz and compensates the phase above 10 Hz.

$$C_{sumFF}(s) = G_{sum}(s)P^{-1}_{sumSn}(s) = \frac{a_3 s^3 + a_2 s^2 + a_1 s + a_0}{N_g[J_L D_s s^2 + (J_L K_s + D_s D_L)s + K_s D_L](\tau_{sum} s + 1)}, \quad (10)$$

$$G_{sum}(s) = \frac{1}{(\tau_{sum} s + 1)}, \quad (11)$$

where $G_{sum}(s)$ is the transfer function that shows the characteristics after nominalization. If there are no modeling errors or disturbances, $T_{sumds} = G_{sum}(s)T^*_{sumds}$.

B. Feedback controller

The feedback controller uses drive shaft rotation speed which is calculated as the following equation.

$$\omega_{sumds} = \frac{\omega_{sumM}}{N_g}. \quad (12)$$

The command value of drive shaft rotation speed is given through the nominal model of $P_{sumMn}(s)$.

$$\omega^*_{sumds} = \frac{P_{sumMn}(s)}{N_g} T^*_{sumff} = \frac{N_g[J_L s^2 + (D_L + D_s)s + K_s]}{a_3 s^3 + a_2 s^2 + a_1 s + a_0} T^*_{sumff}. \quad (13)$$

$H(s)$ is a band-pass filter consists of a low-pass filter and a high-pass filter shown in the following equation.

$$H(s) = \frac{1}{\frac{1}{2\pi f_L}s + 1} \cdot \frac{\frac{1}{2\pi f_H}s}{\frac{1}{2\pi f_H}s + 1}, \quad (14)$$

where f_L is the low-pass frequency, f_H is the high-pass frequency.

The feedback controller is designed with the Nyquist plot shown in Fig. 9. The sensitivity function is an important index for the disturbance suppression characteristics, which is the reciprocal number of the distance between the Nyquist plots and the (−1, 0j) point. If the distance is greater than 1, the disturbance will be suppressed. On the other hand, if it is less than 1, the disturbance will be amplified. To suppress the disturbance, the controller should be designed so that the Nyquist plots is in the direction away from the (−1, 0j) point. As shown in Fig. 9(a), the proportional (P) control without filter has a high magnitude below 2 Hz, which will suppress the slip ratio to nominal slip ratio $\lambda_n = 0$. However, the slip ratio suppressing control is not considered in this controller, and it will affect the acceleration performance. Compared with the P control, the P control with band-pass filter $H(s)$ in Fig. 9(b) has a low magnitude below 2 Hz and above 10 Hz. It can suppress the torsional resonance of the drive shaft due to disturbance without any influence on the feedforward control in other frequency bands. On the contrary, the P control with band-pass filter makes the phase delay above 10 Hz becomes severe. To improve this problem, a derivative (D) controller is added to make Nyquist plot away from the (−1, 0j) point by tuning the control parameters of k_p and k_d as shown in Fig. 9(c).

IV. Experiments of vibration suppression controller for TDA-TVD

In this section, the effect of the drive shaft vibration suppression controller will be confirmed by a half-throttle acceleration experiment on a straight dry path with different control parameters.

Fig. 10. Experimental vehicle equipped with TDA-TVD. TDA-TVD drives rear wheels using two electric motors.

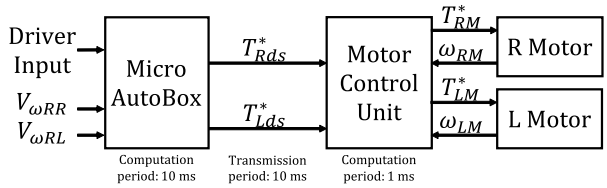

Fig. 11. Experimental vehicle control system.

A. Experimental vehicle

Fig. 10 and Fig. 11 show the experimental vehicle equipped with TDA-TVD unit and the control system. TDA-TVD drives rear wheels using two electric motors. The driving control unit uses MicroAutoBox (MAB) to output drive shaft torque command which is determined by accelerator opening degree and vehicle speed. MAB communicates with Motor Control Unit (MCU) by Controller Area Network (CAN) in a cycle of 10 ms. The proposed controller is implemented on the MCU and calculates the torque command in a cycle of 1 ms. The parameters of experimental vehicle are shown in TABLE I.

B. Experimental conditions

The experimental validation is conducted on a straight dry path, and the steering angle is held at 0 degree by a driver in the whole experiment. The experimental vehicle accelerates from about 20 km/h which is operated by driver using accelerator. The feedforward controller C_{sumFF} is implemented with the experimental parameters and $\tau_{sum} = 1/(2\pi \times f_{sum})$, where $f_{sum} = 10$ Hz.

C. Experimental results

Fig. 14 and Fig. 15 show the results of experimental validation with different control parameters. Where the blue line is the drive shaft torque command, the green line is the motor torque command (converted to shaft side), the red line is the measured drive shaft torque. As shown in Fig. 15 (a), the drive shaft torque vibrates at 6 Hz without control (Motor torque command $T^*_{sumM} = T^*_{sumds}/N_g$) when the vehicle accelerates or decelerates suddenly. It is caused by the torsional resonance of drive shaft. For suppressing the vibration of drive shaft, the proposed controller is implemented in the MCU of experimental vehicle. At first, the parameter of k_p is tuned from 0.2 to 8 with $k_d = 0$ and a band-pass filter of 4 Hz to 8 Hz. The accelerator opening degree is about 25% in this condition. As shown in Fig. 14, the vibration of drive shaft is suppressed when accelerating. The accelerating performances

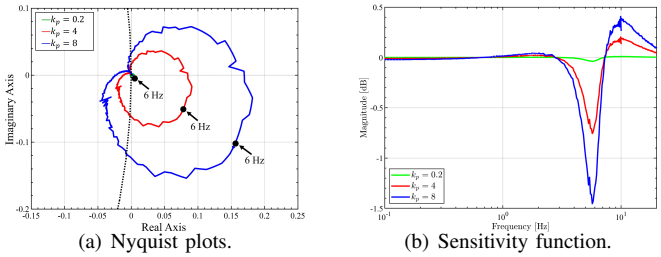

(a) Nyquist plots. (b) Sensitivity function.

Fig. 12. Nyquist plots and sensitivity function with different k_p. The effect of disturbance in 6 Hz becomes smaller when the value of k_p becomes bigger.

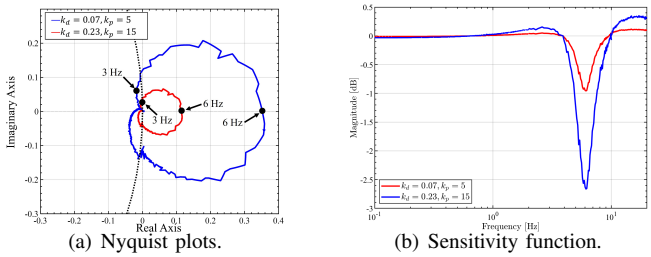

(a) Nyquist plots. (b) Sensitivity function.

Fig. 13. Nyquist plots and sensitivity function of controller with different k_p, k_d. The effect of disturbance in 6 Hz is smaller when $k_p = 0.23$, $k_d = 15$. but it is bigger in 3 Hz.

with different k_p are almost the same because modeling error of feedforward controller is small when accelerating on the dry road surface. Nevertheless, the decelerating performance is different when k_p changes, especially the torsional resonance of drive shaft torque occurred when $k_p = 0.2$. By increasing the value of k_p, the vibration of drive shaft torque and became smaller. It is because the sensitivity function of 6 Hz becomes smaller, which can be confirmed by the distance between the Nyquist plots of 6 Hz and the $(-1, 0j)$ point in Fig. 12.

As mentioned in the previous section, there is phase delay above 10 Hz in P control with band-pass filter, which will affect the disturbance suppression characteristics in this frequency band. The D controller is added to compensate the phase and the band-pass filter is changed to 5 Hz to 7 Hz. The accelerator opening degree is about 20% in this condition. As shown in Fig. 15 (c), There is no influence on accelerating performance when adding the D controller. However, the drive shaft torque vibrates in about 3 Hz to 4 Hz when k_p changes to 15 with $k_d = 0.23$. It is because the effect of modeling error and disturbance became bigger in this frequency band according to the sensitivity function, which can be confirmed in Fig. 13. For decreasing the influence of modeling error and disturbance in this frequency band, the parameters of controller are changed to $k_d = 0.07$, $k_p = 5$. Comparing the experimental results in Fig. 15 (b) and (a), the vibration of drive shaft is suppressed successfully in both accelerating and decelerating conditions.

V. Conclusion

In this paper, a drive shaft vibration suppression controller is designed with frequency domain analysis of the TDA-TVD model. The proposed controller consists of a feedforward controller using the summation inverse model of TDA-TVD, and a feedback controller using the rotation speed of motor.

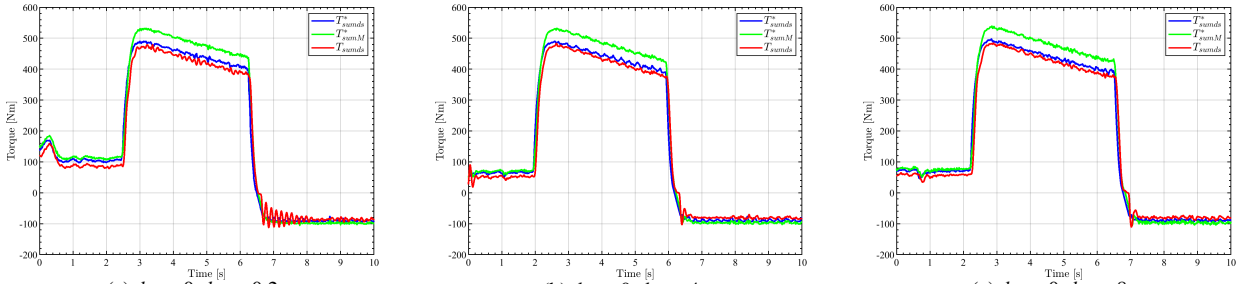

(a) $k_d = 0$, $k_p = 0.2$ (b) $k_d = 0$, $k_p = 4$ (c) $k_d = 0$, $k_p = 8$

Fig. 14. Experimental results of drive shaft torque with different k_p. The acceleration performance are almost the same because modeling error of feedforward controller is small. However, the decelerating performance are different because the effect of modeling error and disturbance in 6 Hz becomes smaller when the value of k_p becomes lager.

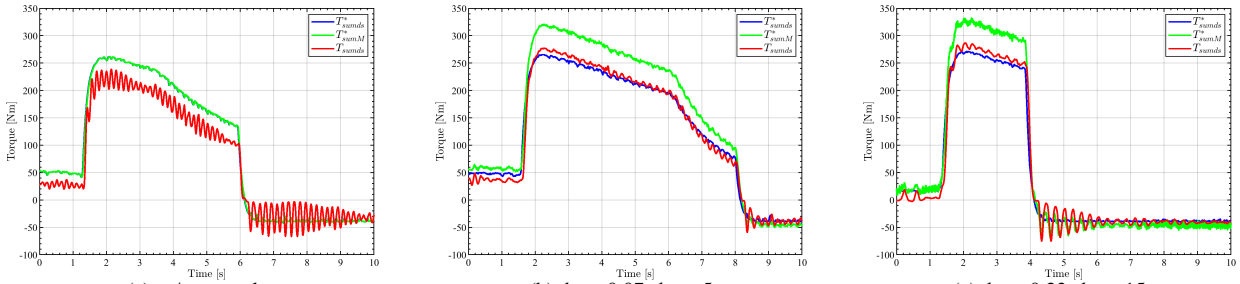

(a) w/o control (b) $k_d = 0.07$, $k_p = 5$ (c) $k_d = 0.23$, $k_p = 15$

Fig. 15. Experimental results of drive shaft torque with different k_d, k_p. Compared with experimental result without control, the vibration of drive shaft with control is suppressed successfully in both accelerating and decelerating conditions. The vibration of drive shaft becomes bigger when decelerating with $k_d = 0.23$, $k_p = 15$ because the magnitude of sensitivity function in 3 Hz becomes big.

To suppress the vibration caused by disturbance and modeling error, the control parameters of k_p and k_d are tuned to make the Nyquist plot away from the $(-1, 0j)$ point. According to the experimental evaluation result of the proposed controller, an improved vibration suppression effect is obtained on both acceleration and deceleration conditions. However, the controller can only be used in translation motion with summation mode. For yaw motion control, the controller based on differential mode should be designed and experimented in in future research.

References

[1] Y. Hori, "Future Vehicle Driven by Electricity and Control-Research on Four-Wheel-Motored " UOT Electric March II "", *IEEE Transactions on Industrial Electronics*, vol.51, no.5, pp.954-962, 2004.

[2] D. Savitski, V. Ivanov, K. Augsburg, T. Emmei, H. Fuse, H. Fujimoto, and L. M. Fridman, "Wheel Slip Control for the Electric Vehicle With In-Wheel Motors: Variable Structure and Sliding Mode Methods", *IEEE Transactions on Industrial Electronics*, vol.67, no.10, pp.8535-8544, 2020.

[3] K. Sawase, M. Chiba, " Study of Lateral Torque-vectoring Differential Suitable for Electric Powered Vehicles ", *Transactions of Society of Automotive Engineers of Japan*, Vol.45, No.5, pp.823-828, 2014 (In Japanese).

[4] E. Katsuyama, "Improvement of ride comfort by triple skyhook control", in Proc. of 9th International Munich Chassis Symposium, pp.215–234, 2018.

[5] T. Suzuki, M. Mae, T. Takeuchi, H. Fujimoto, and E. Katsuyama, " Model-based Filter Design for Triple Skyhook Control of In-Wheel Motor Vehicles for Ride Comfort ", *IEEJ Journal of Industry Applications*, Vol.10, No.3, pp.310-316, 2021.

[6] V. Ivanov, D. Savitski, J. Orus, J. M. R. Fortun, A.Sorniotti, and P. Gruber, " All-wheel-drive electric vehicle with on-board motors: Experimental validation of the motion control systems ", in Proc. of IECON 2015-41st Annual Conference of the IEEE Industrial Electronics Society, pp.001729–001734, 2015.

[7] M. Ravichandran, J. Doering, R. Johri, and K. Rubyal, " Design and evaluation of EV drivetrain clunk and shuffle management control system ", in Proc. of 2020 American Control Conference (ACC), 2020.

[8] T.Karikomi, K.Ito, H.Kawamura and T.Kume, "Highly-responsive acceleration control for the newly developed EV ", in Proc. of JASE Annual Congress(Spring), 20115197, pp.5–8, 2012.

[9] H. Sumiya and H. Fujimoto, " Driving Force Control Method Using Suppression Control of Driving-shaft Vibration for Electric Vehicle with On-board Motor", in Proc. of IEEJ Industry Applications Society Conf, No.106, pp.115–120, 2012 (in Japanese).

[10] J. Amada and H. Fujimoto, " Driving Force Control Method with Resonance Suppression for Drive Shaft of Electric Vehicle with on-boared Motor", in Proc. of IEEJ Technical Meeting Record, IIC-13-003, pp.13-18, 2013 (In Japanese).

[11] H. Fuse, H. Fujimoto, K. Sawase, N. Takahashi, R. Takahashi, Y. Okamura and R. Koga, " Derivation of Dynamic Model of Two-Input-Two-Output Torque Difference Amplification Motor Drive System and Independent Left-and-Right Wheel Control with Decoupling Compensator", *IEEJ Journal of Industry Applications*, Vol.11, No.3, pp.427-436, 2022.

[12] H. Fuse, " Comprehensive Modeling of Drive System and Design of Independent Left-and-Right Wheel Control for Electrified Vehicles ", The University of Tokyo Graduate School of Frontier Sciences Doctoral Dissertation, 2022.

[13] K. Sawase, T. Kikuchi, Y. Fujiwara and T. Furuichi, " Classification and Analysis of Torque-vectoring Differentials with Torque Difference Amplification Mechanism ", *Transactions of Society of Automotive Engineers of Japan*, Vol.48, No.2, pp.317-322, 2017 (In Japanese).

[14] S. Wakui, T. Emmei, H. Fujimoto, and Y. Hori, "Gear collision reduction of geared in-wheel-motor by effective use of load-side encoder", in Proc. of 45th Annu. Conf. IEEE Ind. Electron. Soc., pp.3615–3620, 2019.